Max-Planck-Institut für Meteorologie

REPORT No. 216

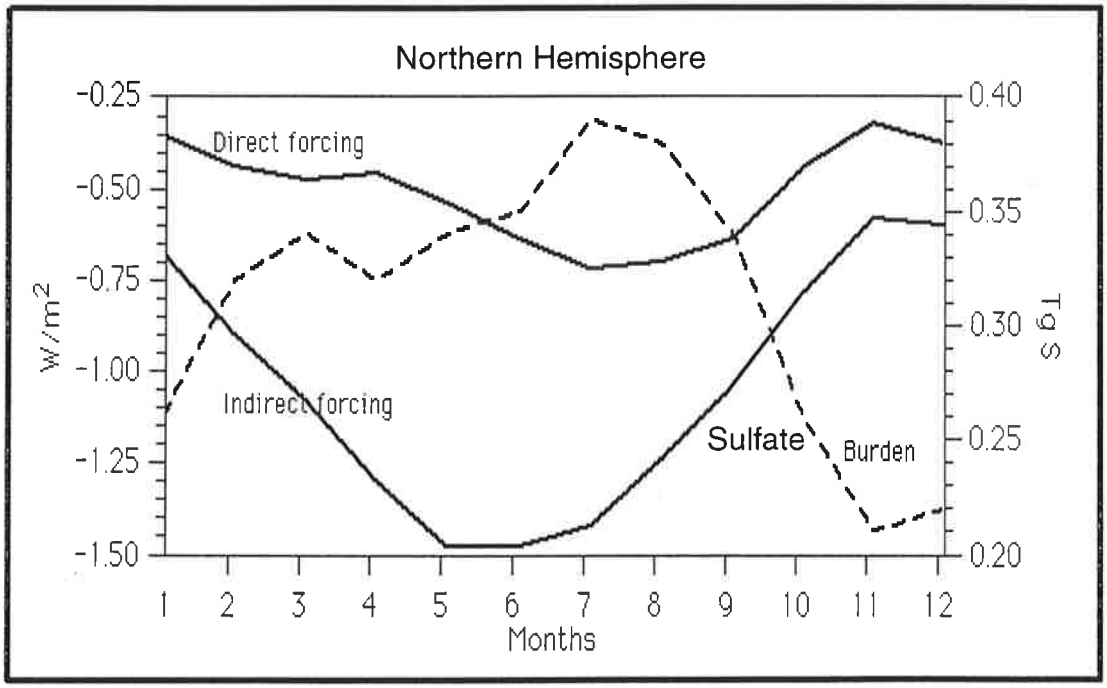

THE ATMOSPHERIC SULFUR CYCLE IN ECHAM-4 AND ITS IMPACT ON THE SHORTWAVE RADIATION

by

Johann Feichter • Ulrike Lohmann • Ingrid Schult

HAMBURG, September 1996

AUTHORS:

Johann Feichter
Ulrike Lohmann
Ingrid Schult

Max-Planck-Institut
für Meteorologie

MAX-PLANCK-INSTITUT
FÜR METEOROLOGIE
BUNDESSTRASSE 55
D - 20146 HAMBURG
GERMANY

Tel.: +49-(0)40-4 11 73-0
Telefax: +49-(0)40-4 11 73-298
E-Mail: <name> @ dkrz.de

The Atmospheric Sulfur Cycle in ECHAM-4 and its Impact on the Shortwave Radiation

Johann Feichter, Ulrike Lohmann and Ingrid Schult
Max-Planck-Institute for Meteorology,
Bundesstrße 55,
D-20146 Hamburg, Germany

September 1996

ISSN 0937 - 1060

Abstract

The atmospheric general circulation model ECHAM-4 is coupled to a chemistry model to calculate the sulfate mass distribution and the radiative forcing due to sulfate aerosol particles. The model simulates the main components of the hydrological cycle and, hence, it allows an explicit treatment of cloud transformation processes and precipitation scavenging. Two experiments are performed, one with pre-industrial and one with present-day sulfur emissions. In the pre-industrial emission scenario SO_2 is oxidized faster to sulfate and the in-cloud oxidation via the reaction with ozone is more important than in the present-day scenario. The atmospheric sulfate mass due to anthropogenic emissions is estimated as 0.38 Tg sulfur. The radiative forcing due to anthropogenic sulfate aerosols is calculated diagnostically. The backscattering of short-wave radiation (direct effect) as well as the impact of sulfate aerosols on the cloud albedo (indirect effect) is estimated. The model predicts a direct forcing of -0.35 W m^{-2} and an indirect forcing of -0.76 W m^{-2}. Over the continents of the northern hemisphere the direct forcing amounts to -0.64 W m^{-2}. The geographical distribution of the direct and indirect effect is considerably different. Whereas the direct forcing is strongest over highly polluted continental regions, the indirect forcing over sea exceeds that over land. It is shown that forcing estimates based on monthly averages rather than on instantaneous sulfate pattern overestimate the indirect effect but have little effect on the direct forcing.

1. Introduction

Recently much attention has been paid to the possibility that sulfate aerosols produced by fossil fuel combustion can cause the atmosphere to cool, thus counteracting greenhouse warming [*Charlson et al.*, 1991; *IPCC*, 1994]. The motivation for these studies was the disparity between the expected temperature rise and the actual observed global mean temperature. In recent decades, the southern hemisphere (SH) surface temperatures appear to have risen more than in the northern hemisphere (NH), where most of the anthropogenic sulfur emissions occur [*Wigley*, 1989]. Additionally, temperature anomalies between 1947 and 1986 [*Jones et al.*, 1988] show highly structured patterns in the NH compared to the SH [*Schwartz*, 1990]. The variations of temperature anomalies suggest a regional forcing. In contrast to most greenhouse gases, which are long-lived (> 10 yrs) and therefore well-mixed within the troposphere, aerosol particles have a life-time in the order of days in the lower troposphere. Therefore the concentrations of aerosols are highly variable in space and time.

Anthropogenic aerosol sources have increased significantly over the past century. Sulfate is possibly the dominant contributor to aerosol radiative forcing, although the effects of other anthropogenic aerosols cannot be discounted. Industrial sulfur emissions have grown by a factor of two since 1950 [IPCC, 1995]. Sulfate is the end product in a complex chain of chemical and physical processes that convert gaseous sulfur species from natural and anthropogenic sources into sulfate. It either forms new particles by condensation (homogeneous nucleation) or condenses on pre-existing particles. Anthropogenic emissions, which account for about 60 - 80% of all non-sea-salt sulfur emissions, occur mainly as SO_2. About 50% of the SO_2 is removed by dry deposition at ground level and by rain [*Langner and Rodhe*, 1991; *Pham et al.*, 1995; *Chin et al.*, 1996]. Of the remaining 50%, the smaller fraction oxidizes to sulfate in the gaseous phase and the larger one is formed via heterogeneous processes within clouds in the aqueous phase. The oxidation rate depends not only on cloud parameters but also on the sulfate concentration itself as an increase in sulfate enhances the acidity of cloud droplets and in turn reduces the dissolution of SO_2 as well as the oxidation rate with ozone. Additionally, sulfate particles are quite efficiently scavenged by cloud water and removed by precipitation. Hence, the sulfate formation rate depends on solar irradiance, concentrations of ambient gases and on meteorological parameters such as cloud cover, liquid water content and the chemical composition of the cloud droplets. Since chemistry models only crudely represent these processes, sulfate formation rates as estimated in previous studies

vary considerably. For example, estimates of the fraction of sulfate formed within clouds ranges between 66% [*Feichter et al.*, 1996] and 90% [*Pham et al.*, 1995] of the total sulfate formation rate. A comparison of model-calculated sulfate concentrations [*WCRP*, 1995] has shown that models produce significantly different vertical sulfate distributions, even though the surface concentrations are in good agreement. Unfortunately, only surface observations of sulfate aerosol concentrations are available. But there are nearly no measurements in the free troposphere .

Sulfate aerosols exert a cooling effect directly by scattering solar radiation back to space and indirectly by changing the optical properties of water clouds. Sulfate aerosols act as cloud condensation nuclei (CCN). An increase of CCN produces higher cloud droplet number concentrations (CDNC). Assuming that the liquid water content remains the same, an increase in CDNC yields smaller cloud droplet radii. This increases the scattering of solar radiation within the cloud and thus the cloud albedo. Low marine clouds in the NH are observed to have smaller droplets and higher albedo than those in the SH [*Han et al.*, 1994]. As formation of precipitation in warm clouds is much more efficient for clouds with fewer but larger droplets, an increase in CCN may also reduce the precipitation efficiency and increase the life-time of clouds [*Albrecht*, 1989]. Obviously sulfate formation and removal strongly influences cloud and precipitation processes and vice versa. Whereas the forcing by greenhouse gases is relatively uniform, the sulfate aerosol forcing shows marked maxima near the main source regions [*Charlson et al.*, 1991; *Kiehl and Briegleb*, 1993] and is highly variable in time due to the episodic nature of the atmospheric sulfate load [*Benkovitz et al.*, 1994]. Additionally, the radiative aerosol forcing varies depending on the solar insolation and the surface albedo. Furthermore, sulfate cooling is restricted to daylight hours, whereas at night sulfate-augmented clouds may increase greenhouse warming and lead to a decline in the diurnal temperature range at surface level [*Balling and Idso*, 1992]. A further complication is the fact that the optical properties of aerosols depend on the chemical composition and size distribution of the particles. These in turn are determined by meteorological parameters such as wind, humidity, cloud and precipitation processes. Lelieveld and Heintzenberg [1992] have shown that the particle size distribution of sulfate aerosols formed in the aqueous-phase is narrower, but has larger radii compared to particles formed in the gas-phase.

Most of the studies so far have estimated the direct effect of anthropogenic sulfate aerosols based only on an annual mean sulfate burden derived by Langner and Rodhe [1991]. The first estimation of the spatial distribution of the direct radiative sulfate forcing was reported by Charlson et al.

[1991]. They found an annual mean global forcing of -0.6 W m^{-2}. Other estimations of the direct effect range from -0.3 W m^{-2} [*Kiehl and Briegleb*, 1993] to -0.9 W m^{-2} [*Taylor and Penner*, 1994]. Differences are mainly due to the treatment of the effects of humidity and to the use of different extinction coefficients. Taylor and Penner [1994], who coupled sulfur chemistry with a climate model, found distinct regional patterns of both the forcing and the temperature response. The forcing from the indirect effect is by far more uncertain because the interactions between aerosols, CCN and cloud optical properties are not well understood. Two climate model studies of the indirect forcing have been conducted that estimate a global average forcing in the range from -0.5 to -1.5 W m^{-2} [*Jones et al.*, 1994; *Boucher and Lohmann*, 1995].

Previous studies of the global sulfur cycle performed with chemical transport models, which do not treat cloud physical processes, fail to account for the complex interaction between sulfate formation and clouds. We took a first step by coupling a chemistry model with an atmospheric circulation model and estimating the direct forcing and the increase in cloud albedo due to anthropogenic sulfate aerosols. In particular, we discuss changes in the oxidation pathways and in the resulting sulfate distributions between pre-industrial and present sulfur emissions.

For the estimate of climate forcing it is probably important to consider the instantaneous spatial sulfate pattern rather than just seasonal averages. To study this effect we performed an experiment with prescribed monthly mean sulfate distributions and compared the resulting forcing with that calculated based on instantaneous sulfate values.

This paper is structured as follows: Section two describes the meteorological and the chemical model. The experiments and the method of the forcing calculations are outlined in section three. In section four we discuss the calculated distribution of the sulfate mass, changes in the importance of the oxidation pathways of SO_2 between a present-day and a pre-industrial emission scenario. Then we will compare our results to those from Langner and Rodhe [1991] whose sulfate distributions were used in various studies to estimate the climate impact of sulfate particles. Next we present the direct and indirect forcing and discuss the geographical distribution. In section five the results are discussed and compared with previous studies.

2. Model description

2.1 The meteorological model

In this study we used the 4th generation Max-Planck-Institute model, ECHAM-4, which is the most recent in a series evolving from the European Centre for Medium Range Weather Forecasts (ECMWF) model. As the previous ECHAM versions [*Roeckner et al.*, 1992, 1996], ECHAM-4 is based on the primitive equations. Prognostic variables are vorticity, divergence, surface pressure, temperature, water vapor and cloud water. Except for the water components, the prognostic variables are represented by spherical harmonics with triangular truncation at wavenumber 30 (T30). Advection of water vapor, cloud water and chemical species is treated with a semi-Lagrangian scheme [*Williamson and Rasch*, 1989]. A semi-implicit time stepping scheme is employed with a weak time filter. The time step is 30 minutes for dynamics and physics, except for radiation which is calculated at 2-hour intervals. A hybrid sigma-pressure coordinate system is used with 19 irregularly spaced levels up to a pressure level of 10 hPa.

The radiation code has been adopted from the ECMWF model [*Morcrette*, 1991] with a few modifications such as the consideration of additional greenhouse gases (methane, nitrous oxide and 16 CFCs) and various types of aerosols (Tanre's aerosol climatology). The water vapor continuum has been revised to include temperature weighted band averages of e-type absorption and also a band dependent ratio of p-e-type to e-type continuum absorption [*Giorgetta and Wild*, 1995]. The single scattering properties of cloud droplets and approximately "equivalent" ice crystals are derived from Mie theory with suitable adaptation to the broad-band model [*Rockel et al.*, 1991]. The effective radius of droplets and ice crystals is parameterized in terms of the liquid and ice water content, respectively.

A high-order closure scheme is used to compute the turbulent transfer of momentum, heat, moisture and cloud water within and above the atmospheric boundary layer. The eddy diffusion coefficients are calculated as functions of the turbulent kinetic energy which is obtained from the respective rate equation [*Brinkop and Roeckner*, 1995]. Vertical fluxes in convective clouds are calculated using the mass flux scheme for penetrative, shallow and mid-level convection developed by Tiedtke [1989] and modified by Nordeng [1995].

The cloud water content is calculated from the cloud water transport equation including sources and sinks due to phase changes and precipitation formation by coalescence of cloud droplets and gravitational settling of ice crystals. Fractional cloud cover is parameterized as a function of rela-

tive humidity [*Roeckner*, 1995; *Sundqvist*, 1978].

ECHAM has been extensively applied and validated in climate studies (Barnett et al., 1989; Cess et al., 1990; Barnett et al., 1991; Latif et al., 1990; Bengtsson et al., 1994; Lohmann and Roeckner, 1995; Lohmann et al., 1995; Wild et al., 1996). Since clouds dominate the sulfur chemistry as well as the radiative energy transfer, we will shortly discuss the performance of ECHAM-4 in terms of cloud cover and cloud liquid water content.

The calculated cloud liquid water path over the oceans has been evaluated with retrievals from microwave observations (SSM/I) by Chen and Roeckner (1996b). The main pattern and magnitude of the space-time distribution is reasonable well reproduced by ECHAM-4 and is within the range of the retrievals by Greenwald et al. (1993) and Weng and Grody (1994). However, differences in the current cloud liquid water path retrievals amounts to a factor of 1.5 globally and to a factor of 2 regionally. The major differences of the model's cloud liquid water path compared to the observations are a lack of contrast between the subtropics and the mid-latitudes and a failure in capturing the observed summer local maxima in the subtropical eastern ocean basins.

Chen and Roeckner (1996a) compare the model's radiation budget with the satellite derived Earth Radiation Budget Experiment data. The model simulations agree with the observed spatial and seasonal distribution of the radiation budget. There are, however, biases, the most serious ones in the short-wave cloud forcing. In the ECHAM-4 model, the short-wave cloud forcing is too large throughout the year in convectively active areas over the tropical oceans but too small over the mid-latitude oceans during summer. The errors in the tropics may be related to the neglect of sub-grid scale cloud water content variability. The bias over the mid-latitude oceans is very likely caused by insufficient cloudiness in these regions, particularly by a lack of low-level clouds.

Although some deficiences remain, the simulated climatological mean and space-time variation of the hydrological cycle is in reasonable agreement with the available observations.

2.2 The sulfur cycle model

Transport, dry and wet deposition and chemical interactions of the chemical constituents are calculated on-line in the global circulation model, ECHAM-4. The model treats three sulfur species as prognostic variables: Dimethyl sulfide (DMS) and sulfur dioxide (SO_2) as gases and sulfate (SO_4^{2-}) as aerosol. Advective transport of these species as well as vertical exchange in the bound-

ary layer and in convective clouds are handled in the same way as the transport of water vapor. The dry deposition flux to the ground is assumed to be proportional to both the concentration in the lowest model layer (30 m above ground) and to a prescribed dry deposition velocity. The dry deposition velocity for SO_2 is assumed to be 0.6, 0.8 and 0.1 cm s^{-1} over land,water and snow, respectively, whereas sulfate aerosols are deposited by a constant velocity of 0.2 cm s^{-1} [*Feichter et al.*, 1996]. Precipitation scavenging of SO_2 and SO_4^{2-} is calculated explicitly in terms of the model's local precipitation formation rate, following a scheme by Giorgi and Chameides [1986]. The performance of this scheme was successfully tested using the aerosol-like radionuclides lead-210 and beryllium-7 [*Brost et al.*, 1991; *Feichter et al.*, 1991].

DMS as well as SO_2 in the gaseous phase are oxidized by reaction with hydroxyl (OH) during the day. Additionally, DMS reacts with nitrate radicals (NO_3) at night. We have assumed that the only end product of DMS oxidation is SO_2. Dissolution of SO_2 within cloud water is calculated according to Henry's law. In the aqueous phase we consider oxidation of SO_2 by hydrogenperoxide (H_2O_2) and ozone (O_3). Three-dimensional monthly mean oxidant concentrations are prescribed based on calculations with ECHAM and a more comprehensive chemical model [*Roelofs and Lelieveld*, 1995]. The calculation of the reaction rates, and of the dissolution and dissociation rates of SO_2, requires assumptions about the pH of cloud water. Hence, we diagnostically estimate the cloud water pH as a function of the sulfate concentrations. The end product of the gaseous and the aqueous oxidation of SO_2 is sulfate (SO_4^{2-}) [for a more detailed description see *Feichter et al.*, 1996]. These calculated sulfate concentrations serve as input to determine the aerosol forcing.

The emission scenario shown in Table 1 differs from that used in Feichter et al. [1996] in respect to volcanic and anthropogenic emissions. We consider both natural emissions from biogenic sources and from background volcanic activity as well as anthropogenic emissions from biomass burning, fossil fuel use and industrial activities. All biogenic emissions from the ocean, soils and plants are assumed to occur as DMS whereas volcanic and anthropogenic emissions are assumed to occur as SO_2. Volcanic emissions are geographically distributed according to Spiro et al. [1992] but a higher source strength of 8 Tg (1 Tg $=10^{12}$ g) S per year is taken from Graf et al. [1996]. About 3 Tg are released at the edges of the volcanoes, 3 Tg S at the top of the volcanoes and 2 Tg S are assumed to be injected into the atmosphere between 5 and 8 km altitude [*Graf et al.*, 1996].

Sulfur emissions from biomass burning amounts to 2.5 Tg per year where 90% are assumed to be anthropogenic. The SO_2 source of 66.8 Tg per year due to fossil fuel combustion and industrial activities is from the "Global Emissions Inventory Activity" (GEIA/IGAC) [Benkovitz et al., 1996]. The data-set consists of four seasonal emission inventories and is valid for the year 1985. The global sulfur emission amounts to 96.3 Tg per year of which 72% can be ascribed to anthropogenic sources.

3. Experiments and analyses of direct and indirect forcing

We performed three experiments: The first (EXP1), representing present-day emissions, applied a global sulfur source strength of 96.3 Tg as described above. The second (EXP2), representing pre-industrial emissions, applied a source strength of 27.2 Tg per year. Both experiments were integrated over 5 years with a spinup time of 3 months. We started the simulation with a zero initial tracer concentration for the three species, DMS, SO_2 and SO_4^{2-}, and prescribed monthly mean climatological values of the sea surface temperature. For each time-step we diagnostically calculated the radiative fluxes by adding the model calculated sulfate aerosol number concentration to the model's standard aerosol climatology. The difference between the short-wave fluxes with the additional sulfate aerosols and those with only the aerosol climatology was considered as the sulfate aerosol forcing. The difference between EXP1 (present-day sulfur emissions) and EXP2 (natural emissions) gives us the anthropogenic contribution.

In order to estimate the uncertainty caused by forcing calculations based on average sulfate distributions we conducted an experiment (EXP3) where we calculated the forcing based on monthly mean sulfate distributions as simulated in EXP1. EXP3 was integrated over one year plus 3 months spin-up time with exactly the same meteorology as in EXP1 .

Aerosol optical properties

Since the model provides only the spatial and temporal distribution of the mass of sulfate ions, we have to make some assumptions about particle size distribution and chemical composition. We assumed for dry sulfate aerosols a log-normal size distribution with a mode radius of r_m = 0.07 μm, a geometric standard deviation of 2.03 and a density of ρ_{AP} = 1.7 g cm^{-3} [*Koepke et al.*, 1994]. The density is for a 75% sulfuric acid solution. These values are used to transform the sulfate mass mixing-ratio into particle number concentrations.

Based on Mie-theory the wave-length dependent optical parameters are calculated from their complex refractive indices and characteristic particle size distributions. Since the current version of ECHAM does not include the dependence of the particle size of the ambient humidity, we assumed a constant relative humidity of 80% with r_m 0.118 μm and ρ_{AP} 1.14 g cm^{-3} [*Koepke et al.*, 1994]. Uncertainties due to this assumption will be discussed in section 5. The resulting mass scattering efficiency at a wavelength of 0.55 μm is 3.41 m^2 g^{-1} for dry sulfate. As the dominant chemical form of sulfate aerosols in the troposphere may be ammonium-sulfate and ammonium-bi-sulfate, the aerosol mass associated with sulfate is higher than the mass of sulfate ions. Charlson et al. (CH91) [1991] used a mass scattering efficiency based on observations of 5.0 m^2 g^{-1} sulfate. Kiehl and Briegleb (KB93) [1993] calculated a mass extinction coefficient of 3.0 m^2 g^{-1}. But they multiply their calculated scattering coefficient by a factor which takes into account that only 60% of the aerosol mass is sulfate obtaining the same value as CH91. In order to compare our results with theirs and to take into account the additional aerosol mass chemically bound with sulfate, we have increased our model calculated sulfate mass by a factor 1.46 to adjust our mass scattering efficiency to 5.0 m^2 g^{-1}. This factor is about the ratio of the molecular weight between ammonium-sulfate and sulfate and can therefore also be interpreted as the increase in aerosol mass due to species chemically bounded to sulfate.

The indirect forcing is calculated according to Boucher and Lohmann [1995]. The sulfate aerosol mass is empirically related to the CDNC of water clouds and of the liquid fraction of mixed-phase clouds. It is based on measurements of SO_4^{2-}, cloud condensation nuclei and CDNC taken at various continental ($CDNC^{cont}$) and marine ($CDNC^{mar}$) sites in clean and polluted air, for a variety of weather situations.

$$CDNC^{cont} = 10^6 * 10^{(2.06 + 0.48 \log(SO_4 2-))}$$

$$CDNC^{mar} = 10^6 * 10^{(2.24 + 0.257 \log(SO_4 2-))}$$

Then CDNC is related to the mean volume radius:

$$r_v = (q_l / b * \rho * 0.75 / (\pi * \rho_{water} * CDNC))^{0.333}$$

wher q_l=liquid water content, ρ = air density, b = cloud cover and ρ_{water} = water density. The cloud optical parameters are defined in terms of the effective droplet radius, r_e. Simultaneous measurements of r_v and r_e suggest a linear relationship between the two radii for liquid clouds ($r_e = 1.1\ r_v$) *[Johnson, 1993]*. Thus an increase in sulfate aerosol concentration leads to a decrease in the effective droplet radius.

4. Results

4.1 Sulfate distribution

Table 2 shows the global and NH budgets of sulfate and the deposition and chemical transformation rates of SO_2 for EXP1 and EXP2. The global and annual mean sulfate amount increased from 0.30 Tg S in the pre-industrial scenario to 0.68 Tg S in the present-day scenario. The anthropogenic contribution is assumed to be the difference between both experiments and amounts to 0.38 Tg S globally. Of the anthropogenic contribution 79% is found in the NH, where 89% of anthropogenic emissions occur. The atmospheric sulfate content shows a clear seasonality, being much higher in the NH in July (0.56 Tg S) than in January (0.39 Tg S) in spite of the fact that sulfur emissions in the NH in January are nearly 20% higher than in July. Distributions of the anthropogenic sulfate column burden (B_{SO4}) for January and July are plotted in Fig. 1. B_{SO4} is highest over the main source regions with distinctly higher values in summer than in winter. In NH mid-latitudes B_{SO4} over continents is higher by a factor of two to three in July compared with January. Maximum values are 20 mg m^{-2} over continents whereas the marine burden in the NH is consistently lower than 4 mg m^{-2} in winter and between 4 and 6 mg m^{-2} in summer. Minimum values of B_{SO4} (< 1 mg m^{-2}) are found over the SH oceans.

The vertically accumulated anthropogenic sulfate mass for different regions and months is plotted in Fig. 2. Globally, we find about 50% of the sulfate mass at levels below 800 hPa (ca. 2 km). Over the NH continents about 80% of the sulfate mass is between 900 (1 km) and 700 hPa (3 km). The sulfate amount in July over land is higher by a factor of two compared with January whereas seasonal differences over the ocean and the southern hemisphere are between 15% and 40%.

The most striking features in the calculated sulfate distribution are the high mixing-ratios in sum-

mer compared with those in winter and the more efficient sulfate formation in EXP2 (pre-industrial) compared with EXP1 (present-day). Whereas only 58% of the emitted sulfur is transformed to sulfate and 42% are removed by deposition in EXP1, 73% of emitted sulfur forms sulfate in EXP2 (see Table 2). To understand this behaviour, we have to analyse the processes which govern the atmospheric sulfate concentrations. The rate of sulfate formation depends on vertical exchange processes and subsequent deposition, mainly dry depositon, of sulfur at ground as well as on the oxidation rate. The atmospheric sulfate load is additionally determined by deposition processes, particularly by wet deposition.

The lower sulfur deposition rate in EXP2 is mainly due to the fact that natural emissions, such as SO_2 from volcanoes, are released into higher altitudes or, like DMS from the marine biosphere, are not affected by dry or wet deposition. These will be more likely to be transported into higher levels whereas sulfur from anthropogenic sources emitted at or near the surface is quite efficiently removed, predominantly by dry deposition. The turnover time of SO_2 with 1.6 days in the present-day scenario reflects also the faster deposition compared to 2.0 days in the pre-industrial case. The low atmospheric sulfate content in winter may be attributed to the weak vertical exchange over continents in mid and high latitudes. Here most of the sulfur is trapped in the boundary layer where it undergoes efficient dry deposition. However, since the deposition rate of SO_2 in EXP1 does not differ very much between summer and winter (48% in January, 42% in July in the NH), this explains only a small part of the summer-winter contrast. The main reason for lower sulfate transformation rates in winter is that oxidation at mid and high latitudes is oxidant limited [*Feichter et al.*, 1996]. A further difference between EXP1 and EXP2 is a shift in the importance of the in-cloud oxidation pathways. The lower sulfate concentrations in EXP2 lead to higher cloud water pH-values and these in turn enhances the uptake of SO_2 in cloud droplets resulting in higher in-cloud oxidation rates in EXP2. Furthermore, lower cloud water acidity increases the reaction rate with O_3. Consequently, in EXP1 only 5% of SO_2 are oxidized by O_3 compared to 12% in EXP2 (Table 2). As the higher sulfate production rate in the pre-industrial emission scenario is mainly due to an increase of in-cloud oxidation, it is partly compensated by a faster removal of sulfate through scavenging. This is reflected in the turn-over time of sulfate which is 4.1 days in EXP1 and 3.5 days in EXP2.

These complex interactions between sulfate formation, scavenging and cloud processes empha-

sizes the need to treat transport, cloud physics and cloud chemistry in a consistent way.

Our global sulfate burden of 0.68 Tg S in EXP1 is within the range of the slow and the fast oxidation case (0.55 resp. 0.77 Tg S) calculated by Langner and Rodhe [1991]. The fraction due to anthropogenic emissions is 0.38 Tg S in our estimation and 0.32 Tg S in their slow oxidation case. Our sulfate burden shows a distinct seasonality with a more than 40% higher sulfate burden in July than in January in the NH (see Table I) whereas theirs shows almost no seasonality whatsoever. These differences are due to the fact that Langner and Rodhe (1991) prescribed a constant lifetime of SO_2 due to in-cloud oxidation whereas our sulfate formation rate reflects the seasonal variation of oxidant concentrations and cloud processes.

Since most of the sulfate is formed in clouds and since the atmospheric residence time of sulfate is determined by wet scavenging, uncertainties in the calculated cloud parameters affect the atmospheric sulfate content. In particular, uncertainties in the calculated cloud liquid water amount respectively the turn-over time of cloud water have a strong impact on the sulfate burden. As pointed out in chapter 2.1, ECHAM's liquid water path is in the range of satellite retrievals from Greenwald et al. (1993) and Weng and Grody (1994) which differ in the global mean by about 60%. Hence, we estimate that uncertainties in the calculated sulfate burden are in the same order. The total uncertainty cannot be assessed because we are lacking any observations of the atmospheric sulfate content. Sufficient sulfate observations to evaluate the model results are only available near the surface over US and Europe. Despite of the fact that surface concentrations are not necessarily repesentative for the atmospheric content, we compare in Fig. 3 the simulated sulfate mixing-ratios to regionally and seasonally averaged observations. The agreement is excellent over the eastern US, over northern Europe in summer and fall and over central Europe in spring and summer whereas the model underestimates the mixing-ratios by more than a factor of two in winter over Europe. As discussed in Feichter et al. (1996) sulfate formation in high latitudes in winter is underestimated by the model.

4. 2 The radiative forcing

The direct and indirect forcing is calculated every time-step based on the instantaneous model calculated sulfate mixing-ratios. The difference between the simulation with present-day sulfur sources and that with pre-industrial sources represents the anthropogenic sulfate forcing. Due to

the high sulfate burden over the industrialized regions we find the highest direct forcing over eastern US, over southern Europe and over south-east Asia (Fig. 4). Generally, the forcing is considerably higher in summer than in winter except over south-east Asia where the forcing shows a rather weak seasonality . The highest values of -3 W m^{-2} are found in July over eastern US and central Europe. The forcing over the oceans of the southern hemisphere is between 0 and -0.2 W m^{-2}. Global and hemispheric mean forcing values are shown in Table 3. The global and annual mean anthropogenic direct solar forcing is -0.35 W m^{-2} which is higher by 25% compared with the value of -0.28 W m^{-2} estimated by KB93. The global mean forcing is strongest in August and weakest in December differing by more than a factor of two. In the NH the direct forcing is highest in July and it is by more than a factor of two higher than in November as shown in Fig. 5. The seasonality of the direct forcing behaves exactly like the sulfate burden.

The solar direct forcing of the present-day sulfur emission scenario is -0.57 W m^{-2} averaged over the globe, -0.79 W m^{-2} in the NH and -0.35 W m^{-2} in the SH. The forcing in the NH is higher by a factor of 3.3 in EXP1 compared to EXP2; the NH sulfate content increased by a factor of 2.9 and the emissions by a factor of 3.0.

Fig. 6 shows the monthly mean forcing due to the indirect effect of anthropogenic sulfate aerosols for January and July. In general, the cooling is greatest over regions covered by low-level clouds which are not shielded by mid- or high-level clouds. As our relationship between sulfate mass and cloud droplet radius shows a steeper increase of CDNC with increasing sulfate over sea than over land, the indirect forcing is stronger over marine regions. In particular, an increase in sulfate concentrations is most effective where the pre-industrial sulfate concentrations were low. We find a relatively high forcing in areas with marine stratocumulus, off the coast of North- and South-America throughout the year and in NH polar regions in July. Maximum values of about -5 W m^{-2} occur in January over the Pacific off the Asian coast, over southern Africa and off the coast of Peru and Brasil. In July maxima are up to -4 W m^{-2} over south-east and northeast Asia, over the Atlantic downstream of north-eastern US and over the Barents Sea.

The calculated indirect forcing due to anthropogenic sulfate aerosols is -0.76 W m^{-2} globally. The monthly mean NH indirect forcing in July is higher by a factor of 2 compared with January (see Table 3). The magnitude of the forcing is also significant in the SH, because of the relatively low sulfate burden in the pre-industrial experiment. The effect on cloud albedo is smaller if the CDNC

are high even in the pre-industrial experiment. Therefore, a relatively high forcing is simulated in the SH. The ratio between NH and SH indirect forcing is about 2 while it is 4 for the direct forcing. Also the land-sea distribution of the direct and the indirect forcing shows a different behaviour as shown in Table 5. Whereas the direct forcing is higher over land than over sea , the indirect forcing over sea exceeds that over land by about one third.

5. Discussion

Two studies of the global atmospheric sulfur cycle calculated on-line with a meteorological circulation model, [*Taylor and Penner*, 1994] (TP94) and [*Feichter et al.*, 1996] (F96), and three studies based on off-line models,([*Langner and Rodhe*, 1991] (LR91), [*Pham et al.*, 1995] (P95) and [*Chin et al.*, 1996] (C96), have been carried out (in the following comparison we will discuss results of present-day experiments). The treatment of the chemical transformations and of the removal processes of F96 is exactly the same as in the current study but the anthropogenic emissions in the current study are lower by about 15%. On the other hand we use a more recent version of the ECHAM model with partly modified model physics which simulates precipitation over NH continents in summer more realistically and leads to an enhanced ventilation of the boundary layer (Brinkop and Roeckner, 1995). These changes result in slightly higher sulfate formation rates. The percentage of SO_2 oxidized to sulfate is in the range between 50 and 60% for all models (TP94 have not reported any budgets) whereas the resulting present-day sulfate burdens show larger differences with 0.68 Tg sulfur in the current study compared with 0.80 in P95, 0.77 in LR91 and 0.53 Tg S in C96. LR91 have also reported a slow oxidation case where only 37% of the SO_2 forms sulfate, resulting in a sulfate burden of 0.55 Tg S. The high sulfate burden in the P95 paper may be partly due to the fact that their sulfur emissions are higher by about 25%. Moreover, their in-cloud oxidation is similar to the approach of LR91 not oxidant limited. Differences in the sulfate burden between the other models can be explained by the different treatment of scavenging processes as expressed in the turn-over times which range between 3.9 (C96) and 5.2 (LR91) days. As pointed out above, the main differences between our calculations and LR91, whose sulfate distributions were used by numerous authors to estimate the climate impact of sulfate aerosols, is a stronger seasonality in our study with a higher sulfate burden in summer than in winter. This enhanced summer sulfate burden increases the annual mean forcing compared with estimates based on LR91.

CH91 found a globally averaged forcing of -0.6 W m^{-2} with maxima over the NH continents between -2 and -4 W m^{-2} based on the anthropogenic sulfate burden from LR91 (slow oxidation case). If we apply their method to our annual mean distribution of cloud cover (60%) and B_{SO4}, our forcing is comparable to CH91, as shown in Table 4, but by a factor of two higher than calculated with our radiation code.

A more detailed calculation of the radiative fluxes has been performed by KB93 also with the LR91 sulfate distribution (Table 4). The geographical distribution of their aerosol forcing is similar to that obtained by CH91 but the magnitude of the forcing is smaller by about a factor of two. KB93 attributed this difference to different optical parameters, particularly to the spectral dependence of the specific extinction which CH91 have assumed to be constant. TP94 calculated a global mean forcing of -0.95 W m^{-2} with a fully coupled climate-chemistry model. If they had accounted for the dependence of the extinction on the humidity in the same manner as KB93, the forcing would be reduced on -0.6 W m^{-2} *[IPCC,* 1995]. Hence, current estimates differ by a factor of two. Since we used about the same spectral dependent optical parameters, our calculated direct forcing should be comparable to KB93. In order to account for the different sulfate burden, we use a normalized forcing introduced by Boucher and Anderson [1995] and Nemesure et al. [1995] as the ratio between forcing [W m^{-2}] and B_{SO4} [g m^{-2}]. The normalized forcing for the anthropogenic contribution is -159 W g^{-1} in KB93's calculation and -157 W g^{-1} in the current study.

KB93 have taken into account the dependence of the sulfate particle size of the ambient humidity based on data of the ECMWF whereas in our study constant optical parameters are used, valid for a 80% relative humidity. To estimate the uncertainty due to this simplification we calculated the direct forcing with an external radiation code [*Bakan,* 1982] assuming first a constant relative humidity of 80%, and then using the relative humidity as calculated by ECHAM. Both calculations were performed based on monthly mean anthropogenic sulfate concentrations and monthly mean meteorological parameters. The estimate of the direct forcing for the case where we considered the ambient relative humidity, gives a value lower by 28% compared to the estimate based on a constant humidity of 80%. That means the relative humidity in the boundary layer of the main sulfur source regions is mostly lower than 80%. If we corrected our direct forcing of -0.35 W m^{-2} by this 28%, we got a forcing of -0.25 W m^{-2} and a normalized forcing of 112 W g^{-1}. This com-

pared to KB93 lower normalized forcing may be partly due to the fact that KB93 have distributed all the sulfate in the lowest 1000 m where humidity is higher.

Two climate model studies of the indirect forcing have been performed [*Boucher and Lohmann*, 1995 (BL95); *Jones et al.*, 1994 (J94)]. Both studies used the sulfate distribution from LR91, J94 from the slow oxidation case and BL95 from the fast oxidation case, and related the CDNC empirically to the sulfate mass. The resulting global and annual mean indirect sulfate forcing is -1.26 W m^{-2} (J94) and -1.1 W m^{-2} (BL95) which is higher than our estimate of -0.76 W m^{-2}. Taking into account that the sulfate burden used by BL95 is about 40% higher than that used by J94, the sensitivity of the cloud albedo against changes of the CDNC is much higher in the approach by J94. Since we used the same approach as BL95 and additionally our sulfate burden is higher, differences in the estimate of the forcing may be due to the fact that our pre-industrial sulfate burden is higher than theirs. As pointed out above, the higher the pre-industrial burden the smaller is the effect of an anthropogenic increase on the cloud albedo.

In our study the average indirect forcing over marine areas is slightly higher than over continents. This can be attributed to the different slopes over land and over sea in the relationship between sulfate mass and CDNC as well as to the higher liquid water content of marine clouds. This is in agreement with observations by Platnick and Twomey [1994] who report, based on satellite remote sensing data, a higher cloud susceptibility, defined as the influence of CCN number concentrations on cloud albedo, of marine stratus clouds. The fact that the indirect forcing is relatively high over marine areas compared to continental regions constitutes the main difference in the pattern between direct and indirect forcing.

Estimations of the indirect forcing are much more uncertain than of the direct effect. Besides the uncertainties in determining the fine particle mass, size distribution and chemical composition of the aerosols, the aerosol mass distribution is linked to the CDNC. We use a relationship derived from observations between the sulfate mass and the CDNC [*Boucher and Lohmann*, 1995] assuming that sulfate is a good tracer of the anthropogenic induced increase in CCN. However, measurements over the east coast of the United States and over the northeast Atlantic by Hegg et al. [1995] show that the nucleation of sulfate is not very efficient and that in contrast to the aerosol mass where sulfate dominates, a substantial percentage of the CCN is not sulfate. That means that changes in the sulfate mass will not necessarily result in a comparable change in CCN. Moreover, applying a relationship between sulfate mass and CDNC implies a constant fraction of sulfate to

non-sulfate aerosol mass which is not observed. Additionally, it is assumed that the internal mixture between sulfate ions and other compounds is the same in present and in pre-industrial times.

Benkovitz [1994] emphasized the highly episodic nature of sulfate concentrations as well as of aerosol optical depth. To study the influence of this variability on the forcing and to estimate the uncertainties associated by the use of averaged sulfate concentrations instead of instantaneous values, we performed an experiment where we used the monthly mean sulfate distributions from our present-day emission scenario to calculate the forcing. In this experiment the meteorology is exactly the same as in EXP1. We calculated the difference of the short-wave fluxes at the top of the atmosphere between the experiment with averaged sulfate concentrations and the experiment with the instantaneous values. Generally, calculations with averaged sulfate fields tend to overestimate the forcing. This overestimation is negligible for the direct effect, but it amounts to 20% globally for the indirect effect, which is much stronger affected by averaging due to the non-linear relation between aerosols, clouds and the radiation fluxes. This overestimation is highest off the coasts of polluted continental areas whereas over most of the continents the forcing is slightly underestimated. Differences between sea and land may be due to the fact that changes in the optical depth affects the cloud albedo more if the optical depth is relatively low as is the case for marine clouds. An error of about 20% is small compared with the uncertainty of the relationship between sulfate and CDNC which is estimated to be ± 0.5 W m^{-2} (BL95) but regional differences are in the order of the indirect forcing itself. Differences may even be larger if we had calculated the forcing based on a monthly or annual averaged cloud cover as it was done in most of the previous studies.
This effect explain about 50% of the difference in the calculated indirect forcing between BL95 and our study.

6. Conclusion

We coupled a sulfur chemistry model with an atmospheric GCM and calculated the loss of short-wave radiation due to backscattering of the anthropogenic fraction of sulfate particles as well as its impact on cloud albedo and the radiation balance. The coupling of chemical and meteorological processes allows us to take the non-linear nature of sulfate formation, cloudiness and radiation into account. We performed three experiments: one considering present-day sulfur emissions, one with pre-industrial sulfur emissions and one with prescribed monthly mean sulfate distributions, as

obtained from the present day experiment, to study the effect of the temporal variability of sulfate concentrations on the radiative forcing. The main findings of this study are:

- Sulfur from natural sources, like DMS and SO_2 from volcanic emissions, contributes relatively more effectively to the atmospheric sulfate burden than anthropogenic emissions. This is due to the fact that anthropogenic emissions released near the surface are more likely removed by dry deposition than sulfur species released in higher altitudes. Hence, in the pre-industrial emission scenario 73% of the emitted sulfur is transformed to sulfate compared to 58% in the present-day scenario.
- In the pre-industrial scenario clouds are less acidic due to lower sulfate concentrations which enhances the dissolution of SO_2 in cloud droplets and increases the reaction with O_3. Therefore, in-cloud oxidation of SO_2 to sulfate is more important in the pre-industrial than in the present-day emission scenario.
- The horizontal distribution of the direct radiative forcing due to sulfate particles mainly reflects the sulfur source distribution because the sulfate pre-cursor SO_2 as well as sulfate are quite short-lived. The globally and annually averaged direct forcing of -0.35 W m^{-2} due to anthropogenic sulfur emissions is relatively small compared to the greenhouse gas forcing. However, this does not imply that the effect is negligible as the forcing can regionally be one order of magnitude larger. Over the continents of the NH, where sulfur emissions are highest, the average forcing is with -0.64 W m^{-2} nearly twice as large as the global mean forcing.
- The indirect effect due to changes of the cloud albedo amounts to -0.76 W m^{-2}. The indirect forcing over sea exceeds that over land by 16%. This is in striking contrast to the direct forcing which is higher by 70% over land versus sea. This is due to the fact that marine clouds have a relatively low number of cloud droplets and are therefore more susceptible to changes in the number of CCN. Therefore, the geographical distribution of the direct and the indirect forcing exhibits considerably different pattern.
- Estimates based on average mean sulfate distributions tend to overestimate the forcing. In particular, the indirect effect is strongly affected by averaging due to the non-linear relation between aerosols, clouds and the radiation fluxes. The overestimation of the indirect effect amounts to 20% globally and to more than 100% regionally.

A further step will be to fully couple the chemical and the meteorological model to study the cli-

mate response of such spatially uneven distribution of forcing patterns. However, sulfate is only one chemical compound of the fine particle mass and in order to get a realistic understanding of the aerosol-climate feedback, we have to consider the entire suite of aerosol types as well as to improve the specification of the aerosol growth and the formation of CCN.

References

Albrecht, B.A., Aerosols, cloud microphysics, and fractional cloudiness, *Science*, *245*, 1227-1230, 1989.

Balling, R.C., and S.B. Idso, Climatic change in Britain: Is SO2 more significant than CO2?, *Theor. Appl. Climatol.*, *45*, 251-256, 1992.

Bakan, S., Strahlungsgetriebene Zellullarkonvektion in Schichtwolken, Ph.D.Thesis, University of Hamburg, 1982.

Barnett, T. P., L. Duemenil, U. Schlese, E. Roeckner and M. Latif, The effect of Eurasian snow cover on regional and global climate, *J. Atmos. Sci.*, 46, 661-685, 1989.

Barnett, T. P., M. Latif, E. Kirk and E. Roeckner, On ENSO physics, *J. Clim.*, 4, 487-515, 1991.

Bates, T.S., J.D. Cline, R.H. Gammon, and S.R. Kelly-Hansen, Regional and seasonal variations in the flux of oceanic dimethylsulfide to the atmsophere, *J. Geophys. Res.*, *92*, 2930-2938, 1987.

Bengtsson, L., K. Arpe, E. Roeckner and U. Schulzweida, Climate predictability experiments with a general circulation model, (subm.) Clim. Dyn., 1996.

Benkovitz, C.M., C.M. Berkowitz, R.C. Easter, S. Nemesure, R. Wagener, and S.E. Schwartz, Sulfate over the North Atlantic and adjacent continental regions: Evaluation for October and November 1986 using a three-dimensional model driven by observation-derived meteorology, *J. Geophys. Res.*, *99* (D10), 20,725-20,756, 1994.

Boucher, O., and T.L. Anderson, General circulation model assessment of the sensitivity of direct climate forcing by anthropogenic sulfate aerosols to aerosol size and chemistry, *J. Geophys. Res.*, *100* (D12), 26,117-26,134, 1995.

Boucher, O., and U. Lohmann, The sulfate-CCN-cloud albedo effect: A sensitivity study with two general circulation models, *Tellus*, *47B*, 281-300, 1995.

Brinkop, S., and E. Roeckner, Sensitivity of a general circulation model to parameterizations of cloud-turbulence interactions in the atmsopheric boundary layer, *Tellus*, *47A*, 197-220, 1995.

Brost, R.A., J. Feichter, and M. Heimann, Three-Dimensional Simulation of 7Be in a Global Climate Model, *J. Geophys. Res.*, *96* (D12), 22,423, 1991.

Cess, R.D., G.L. Potter, J.P. Blanchet, G.J. Boer, A.D. Del Genio, M. Déqué, V. Dymnikov, V. Galin, W.L. Gates, S.J. Ghan, J.T. Kiehl, A.A. Lacis, H. Le Treut, Z.-X. Li, X.-Z. Liang, B.J. McAvaney, V.P. Meleshko, J.F.B. Mitchell, J.-J. Morcrette, D.A. Randall, L. Rikus, E. Roeckner, J.F. Royer, U. Schlese, D. A. Sheinin, A. Slingo, A.P. Sokolow, K.E. Taylor, W.M. Washington, R.T. Wetherald, I. Yanai and M.-H. Zhang, Intercomparison and interpretation of climate feedback processes in 19 atmospheric general circulation models, *J. Geophys. Res.*, 95, 16601-16615, 1990.

Charlson, R.J., J. Langner, H. Rodhe, C.B. Leovy, and S.G. Warren, Perturbation of the Northern Hemisphere radiative balance by backscattering from anthropogenic aerosols, *Tellus*, *43AB*, 152-163, 1991.

Chen, C. T. and E. Roeckner, Validation of the Earth radiation budget as simulated by the Max Planck Institute for Meteorology general circulation model ECHAM4 using satellite observations of the Earth Radiation Budget Experiment, *J. Geophys. Res.,* 101, 4269-4287, 1996.

Chen, C. T. and E. Roeckner, Cloud simulations with the Max-Planck-Institute for Meteorology general circulation model ECHAM4 and comparison with observations, Report No. 193, Max-Planck-Institute for Meteorology, Hamburg, Germany, 1996.

Chin, M., D.J. Jacob, G.M. Gardner, M. Foreman-Fowler, and P.S. Spiro, A global three-dimensional model of tropospheric sulfate, *J. Geophys. Res., (submitted)*, 1996.

Feichter, J., R.A. Brost, and M. Heimann, Three-Dimensional Modeling of the Concentration and Deposition of 210 Pb Aerosols, *J. Geophys. Res.*, *96* (D12), 22,447, 1991.

Feichter, J., E. Kjellström, H. Rodhe, F. Dentener, J. Lelieveld, and G.-J. Roelofs, Simulation of the tropospheric sulfur cycle in a global climate model, *Atmos. Environ.*, *30* (10/11), 1693-1707, 1996.

Giorgetta, M., and M. Wild, The water vapour continuum and its representation in ECHAM4, Max-Planck-Institute for Meteorology, Hamburg, Germany, 1995.

Giorgi, F., and W.L. Chameides, Rainout lifetimes of highly soluble aerosols and gases inferred from simulations with a general circulation model, *J. Geophys. Res.*, *91*, 14,367-14,376, 1986.

Graf, H.-F., J. Feichter, and B. Langmann, Volcanic sulfur emissions: Estimates of source strength and its contribution to the global sulfate distribution, *J. Geophys. Res. (acc.)*, 1996.

Greenwald T. J., G. L. Stephens , T. H. Von der Haar, D. L. Jackson, A physical retrieval of cloud liquid water over the global oceans using Special Sensor Microwave/Imager (SSM/I) observations, *J. Geophys. Res.*, 98, 18,471-18,488, 1993.

Han, Q., W.B. Rossow, and A.A. Lacis, Near-global survey of effective droplet radii in liquid water clouds using ISCCP data, *J. Climate*, *7*, 465-497, 1994.

Hao, W.M., M.H. Liu, and P.J. Crutzen, *Estimates of annual and regional releases of CO2 and other trace gases to the atmosphere from fires in the tropics*, 440-462 pp., Springer Verlag, New York, 1990.

Hegg, D. A., Hobbs P. V., Ferek R. J., Waggoner A. P., Measurements of some aerosol properties relevant to radiative forcing on the east coast of the United States, *J. Appl. Meteor.*, 34, 2306-2315, 1995.

IPCC, Climate Change 1994, Radiative forcing of climate change and an evaluation of the IPCC IS92 emission scenarios, Houghton J. T., Filho L. G. M., Bruce J., Lee H., Callander B. A., Haites E., Narris N., Maskell K (Eds.), Cambridge University Press, Cambridge, UK, 1994.

IPCC, Climate Change 1995, The science of climate change, Intergovernmental Panel on Climate Change, Houghton J. T., Filho L. G. M., Callander B. A., Narris N., Kattenberg A., Maskell K (Eds.), Cambridge University Press, Cambridge, UK, 1996.

Johnson, D. W., Parameterization of the cloud topped boundary layer. Aircraft measurements . In: ECMWF workshop proceedings "Parameterization of the cloud topped boundary layer", ECMWF, Reading, UK, 77-117, 1993.

Jones, A., D.L. Roberts, and A. Slingo, A climate model study of indirect radiative forcing by anthropogenic sulphate aerosols, *Nature*, *370*, 450-453, 1994.

Jones, P.D., T.M.L. Wigley, C.K. Folland, and D.E. Parker, Spatial patterns in recent worldwide temperature trends, *Climate Monitor (Univ. of East Anglia, U.K:)*, *16*, 175-185, 1988.

Kiehl, J.T., and B.P. Briegleb, The relative roles of sulfate aerosols and greenhouse gases in climate forcing, *Science*, *260*, 311-314, 1993.

Koepke, P., M. Hess, I. Schult and E. Shettle, Global aerosol data set, Fourth International Aerosol Conference, Los Angeles, U.S.A., August 29 - September 2, 1994.

Langner, J., and H. Rodhe, A global three-dimensional model of the global sulfur cycle, *J. Atmos. Chem.*, *13*, 225-263, 1991.

Latif, M., J. Biercamp, H. v. Storch, M. J. McPhaden, and E. Kirk, Simulation of ENSO related surface wind anomalies with an atmospheric GCM forced by observed SST, *J. Clim.*, 3, 509-521, 1990.

Lelieveld, J., and J. Heintzenberg, Sulfate cooling effect on climate through in-cloud oxidation of anthropogenic SO2, *Science*, *258*, 117-120, 1992.

Lohmann, U. and E. Roeckner, Influence of cirrus cloud radiative forcing on climate and climate sensitivity in a general circulation model, *J. Geophys. Res.*, 100, 16,305-16,323, 1995.

Lohmann, U. and E. Roeckner, Design and performance of a new cloud microphysics scheme developed for the ECHAM general circulation model, *Clim. Dyn.*, 12, 557-572, 1996.

Lohmann, U., E. Roeckner, W. D. Collins, A. J. Heymsfield, G. M. McFarquhar and T. P. Barnett,

The role of water vapor and convection during the Central Equatorial Pacific Experiment from observations and model simulations, *J. Geophys. Res.*, 100, 26,229-26,245, 1995.

Morcrette, J.-J., Radiation and Cloud Radiative Properties in the European Centre Medium Range Weather Forecasts Forecasting System, *J. Geophys. Res.*, *96* (D5), 9121, 1991.

Nemesure, S., R. Wagener, and S.E. Schwartz, Direct shortwave forcing of climate by the anthropogenic sulfate aerosol: Sensitivity to particle size, composition, and relative humidity, *J. Geophys. Res.*, *100* (D12), 26,105-26,116, 1995.

Nordeng, T.E., Extended versions of the convective parameterization scheme at ECMWF and their impact on the mean and transient activity of the model in the tropics, *J. R. Meteorol. Soc.*, *(submitted)*, 1995.

Pham, M., J.-F.M.u.l. Muller, G.P. Brasseur, C. Granier, and G.M.e.g. Megie, A three-dimensional study of the tropospheric sulfur cycle, *J. Geophys. Res.*, *100* (D12), 26,061-26,092, 1995.

Rockel, B., E. Raschke, and B. Weyres, A parameterization of broad band radiative transfer properties of water, ice and mixed clouds, *Beitr. Phys. Atmosph.*, *64*, 1-12, 1991.

Roeckner, E., K. Arpe, L. Bengtsson, S. Brinkop, L. Dümenil, M. Esch, E. Kirk, F. Lunkeit, M. Ponater, B. Rockel, R. Sausen, U. Schlese, S. Schubert, and M. Windelband, Simulation of the present-day climate with the ECHAM model: Impact of model physics and resolution, Max-Planck-Institute for Meteorology, Hamburg, Germany, 1992.

Roeckner, E., Parameterization of cloud radiative properties in the ECHAM4 model. In: WCRP workshop on "Cloud microphysics parameterizations in global atmospheric circulation models", 23-25 May, 1995, WCRP-90, Kananaskis, Canada, 105-116.

Roeckner, E., K. Arpe, L. Bengtsson, M. Christoph, M. Claussen, L. Dümenil, M. Esch, M. Giorgetta, U. Schlese and U. Schulzweida, The atmospheric general circulation model ECHAM-

4: Model description and simulation of present-day climate, Report Max-Planck-Institute for Meteorology, Hamburg, Germany, 1996.

Roelofs, G.-J., and J. Lelieveld, Distribution and budget of O3 in the troposphere calculated with a chemistry general circulation model [O_3], *J. Geophys. Res.*, *100* (D10), 20,983-20,998, 1995.

Schwartz, S.E., Cloud albedo and climate perturbations due to anthropogenic sulfate, in *GLOMAC Workshop*, Scloß Ringberg, Germany, 1990.

Spiro, P.A., D.J. Jacob, and J.A. Logan, Global Inventory of Sulfur Emissions With 1deg x 1deg Resolution, *J. Geophys. Res.*, *97* (D5), 6023, 1992.

Sundqvist, H., A parameterization scheme for non-convective condensation including prediction of cloud water content, Q. J. R. Meteorol. Soc., 104, 677-690, 1978.

Taylor, K.E., and J.E. Penner, Response of the climate system to atmospheric aerosols and greenhouse gases, *Nature*, *369*, 734-737, 1994.

Tiedtke, M., A comprehensive mass flux scheme for cumulus parameterization in large-scale models, *Mon. Wea. Rev.*, *117*, 1779-1800, 1989.

WCRP, Workshop on modelling the transport and scavenging of trace constituents of clouds in global atmospheric models, in *WCRP workshop*, Cambridge, U.K., 1995.

Weng, F., and N. C. Grody, Retrieval of cloud liquid water using the special sensor microwave imager (SSM/I) , *J. Geophys. Res.*, 99, 25,535-25,551, 1994.

Wigley, T.M.L., Possible climate change due to SO2 derived cloud condensation nuclei, *Nature*, *339*, 365-367, 1989.

Wild, M., A. Ohmura, H. Gilgen, and E. Roeckner, Validation of GCM-simulated radiative fluxes using surface observations, *J. Climate*, 8, 1309-1324.

Williamson, D.L., and P.J. Rasch, Two-dimensional semi-Lagrangian transport with shape-

preserving interpolation, *Mon. Wea. rev.*, *117*, 102-129, 1989.

Table 1. Global sulfur emissions in Tg S per year.

Species		Source	Reference	Tg S / yr
Natural	DMS	Marine biosphere	[*Bates et al.*, 1987]	18.1
	DMS	Terrestrial biosphere	[*Spiro et al.*, 1992]	0.9
	SO_2	Volcanoes	[*Spiro et al.*, 1992] [*Graf et al.*, 1996]	8.0
Anthropogenic	SO_2	Biomass burning	[*Hao et al.*, 1990]	2.5
	SO_2	Fossil fuel use and industry	[*Benkovitz et al.*, 1996]	66.8
Total				96.3

Table 2. Global and hemispheric budgets and sink processes of SO_2 in % (oxidation + deposition amounts to 100%) for the scenario with present-day sulfur sources (EXP1) and with pre-industrial sources (EXP2).

		Emission and DMS oxidation [Tg S/ yr] [Tg S/mo]	Sulfate burden [Tg S]	Oxidation of SO_2 [%]			Deposition of SO_2 [%]
				with OH	with H_2O_2	with O_3	
EXP 1	Global annual mean	96.3	0.68	12	41	5	42
	NH Jan.	6.8	0.39	5	40	7	48
	NH July	5.8	0.56	22	35	1	42
EXP 2	Global annual mean	27.3	0.30	12	49	12	27
	NH Jan.	1.1	0.13	10	44	21	25
	NH July	1.2	0.18	16	52	6	26

Table 3. Global and hemisperic mean direct and indirect forcing in W m^{-2}.

		EXP2 (pre-industrial)	EXP1-EXP2 (anthropogenic)	EXP1 (present-day)
Direct annual mean	Global	-0.23	-0.35	-0.57
	NH	-0.24	-0.55	-0.79
	SH	-0.22	-0.13	-0.35
Direct monthly mean	Jan NH	-0.22	-0.40	-0.62
	July NH	-0.24	-0.79	-1.03
Indirect annual mean	Global	-	-0.76	-
	NH	-	-1.04	-
	SH	-	-0.46	-
Indirect monthly mean	Jan NH	-	-0.68	-
	July NH	-	-1.42	-

Table 4. Anthropogenic sulfate burden B_{SO4} [mg SO_4^{2-} m^{-2}], anthropogenic direct forcing [W m^{-2}] and normalized forcing [W g^{-1}] as calculated by Charlson et al. [1991] (CH91), as calculated with the cloud cover and the B_{SO4} of the current study according to Charlson's method (ECHAM-CH), as calculated in the current study (ECHAM) and as calculated by Kiehl and Briegleb [1993] (KB93).

Model	Sulfate burden [mg SO_4^{2-} m^{-2}]	Direct forcing [W m^{-2}]	Normalized forcing [W g^{-1}]
CH91	2.00	-0.60	-300
ECHAM-CH	2.23	-0.67	-300
ECHAM	2.23	-0.35	-157
KB93	1.76	-0.28	-159

Table 5. Annual mean direct and indirect forcing [W m^{-2}] and sulfate burden [mg SO_4^{2-} m^{-2}] due to anthropogenic emissions over land and over sea .

	Direct forcing		Indirect forcing		Sulfate burden	
	Land	Sea	Land	Sea	Land	Sea
NH	-0.64	-0.51	-0.83	-1.19	5.01	2.79
SH	-0.19	-0.12	-0.37	-0.49	1.59	0.75

Figure caption

Figure 1. Monthly mean vertical sulfate column due to anthropogenic emissions in [mg SO_4^{2-} m^{-2}].
Contour lines: 1, 2, 4, 6, 8, 10, 12, 14, 16, 18, 20, 24, 28, 32
a) January
b) July

Figure 2. Vertical accumulated anthropogenic sulfate mass in [mg S m^{-2}] over northern and southern hemisphere oceans and continents.
a) January
b) July

Figure 3. Comparison of observed (solid line) and simulated (dashed line) seasonal variation of sulfate in surface air. Regional averages are calculated for all stations in the EMEP-net (EMEP, 1984) involving 23 gridsquares, 8 gridsquares in central Europe between 44 and 55 degrees north, stations from the NADP-, IMPROVE- and CAPMON-networks in North America, 12 gridsquares in eastern North America between 33 and 50 degrees north, polar and oceanic sites (equatorwards of 30 degrees). Northern Europe consists of 7 gridsquares north of 55 N^o. (Feichter et al., 1996)

Figure 4. Monthly mean direct anthropogenic forcing in [W m^{-2}].
Contour lines: -0.1, -0,5, -1..0, -1.5, -2.0, -3.0, -4.0
a) January
b) July

Figure 5. Monthly mean anthropogenic sulfate burden [Tg S] and direct and indirect forcing [W m^{-2}] on the northern hemisphere.

Figure 6. Monthly mean indirect anthropogenic sulfate forcing [W m^{-2}].
Contour lines: -0.5, -1.0, -2.0, -3.0, -4.0
a) January
b) July

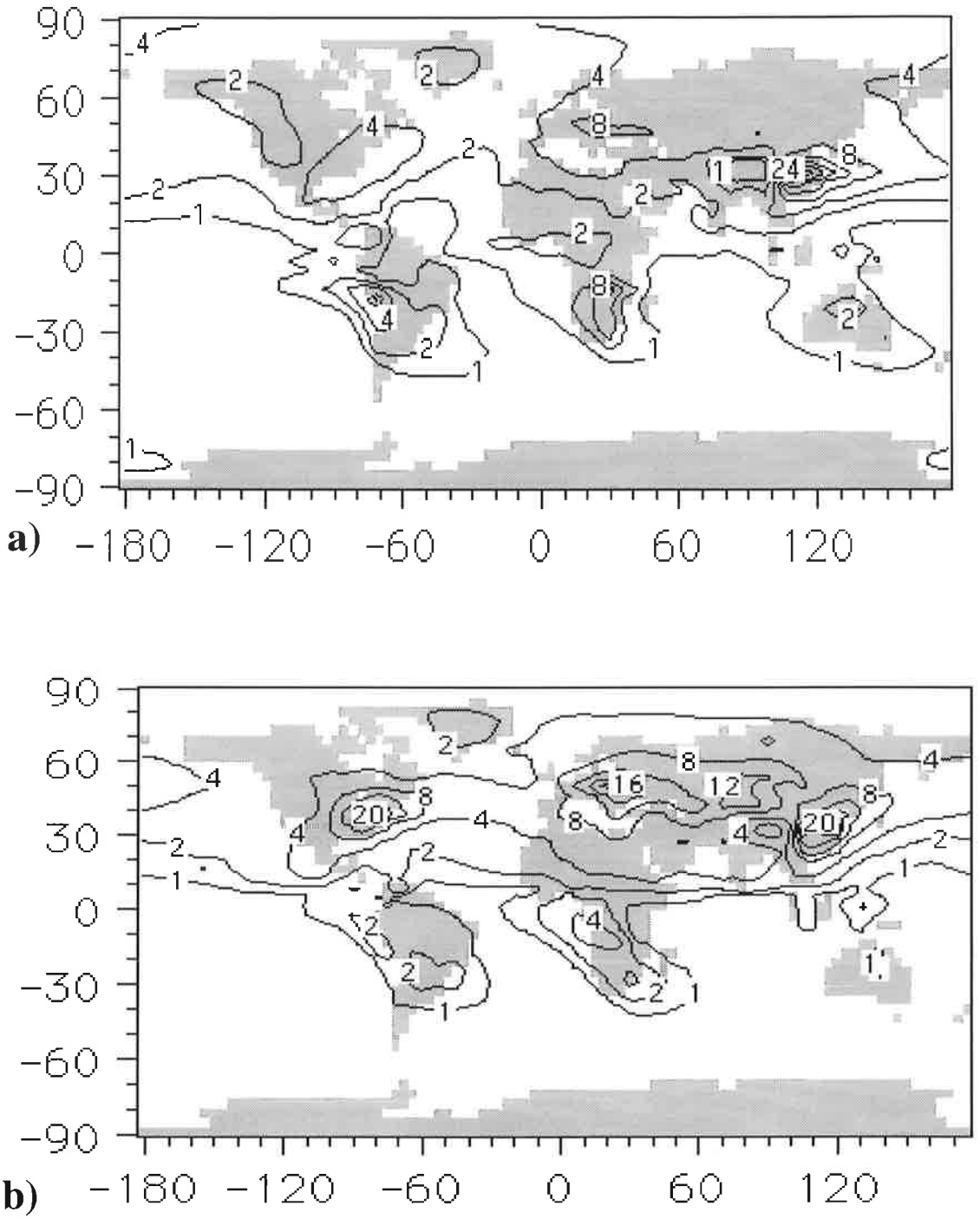

Figure 1. Monthly mean vertical sulfate column due to anthropogenic emissions in [mg SO_4^{2-} m^{-2}].
Contour lines: 1, 2, 4, 6, 8, 10, 12, 14, 16, 18, 20, 24, 28, 32
a) January
b) July

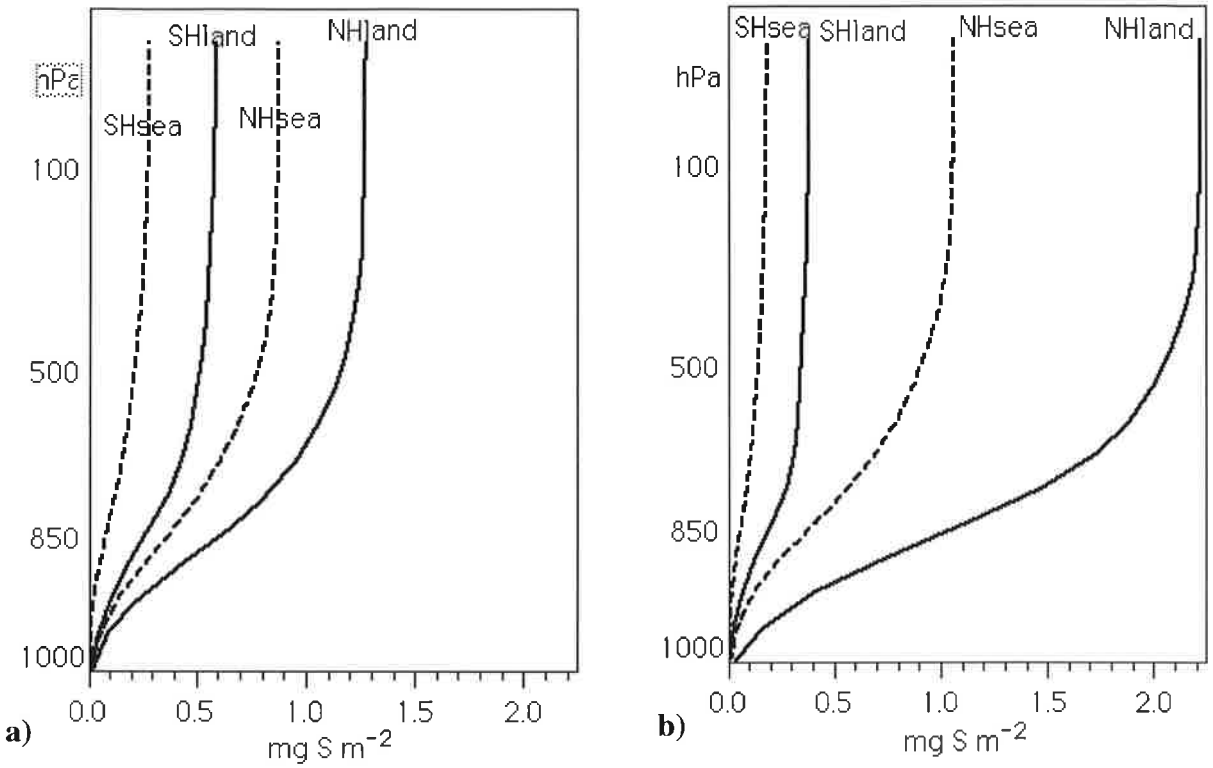

Figure 2. Vertical accumulated anthropogenic sulfate mass in [mg S m^{-2}] over northern and southern hemisphere oceans and continents.
a) January
b) July

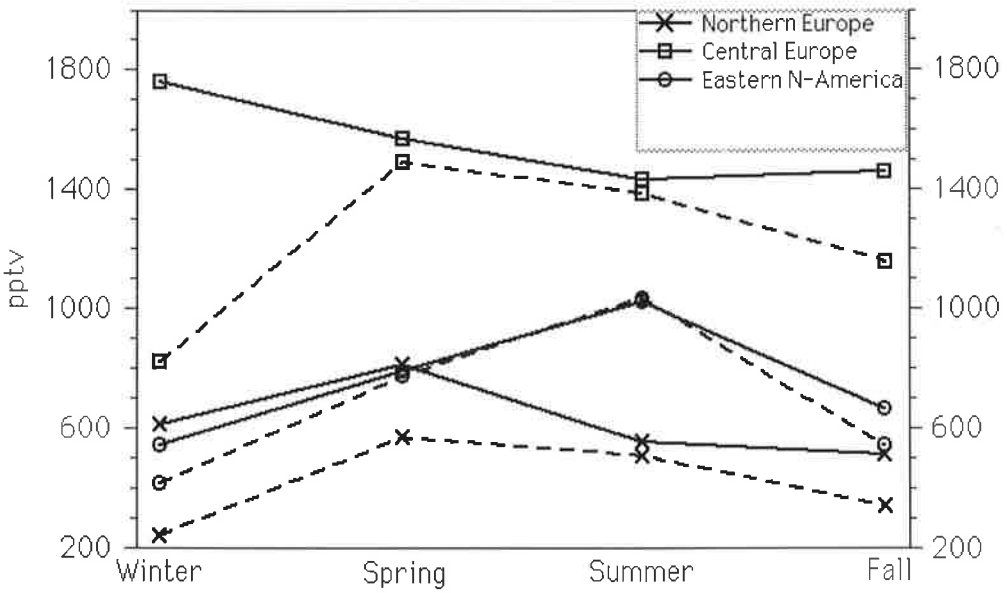

Figure 3. Comparison of observed (solid line) and simulated (dashed line) seasonal variation of sulfate in surface air. Regional averages are calculated for all stations in the EMEP-net (EMEP, 1984) involving 23 gridsquares, 8 gridsquares in central Europe between 44 and 55 degrees north, stations from the NADP-, IMPROVE- (Malm et al. 1994) and CAPMON-networks in North America, 12 gridsquares in eastern North America between 33 and 50 degrees north, polar and oceanic sites (equatorwards of 30 degrees). Northern Europe consists of 7 grid-squares north of 55 N^{o}. (Feichter et al., 1996)

a)

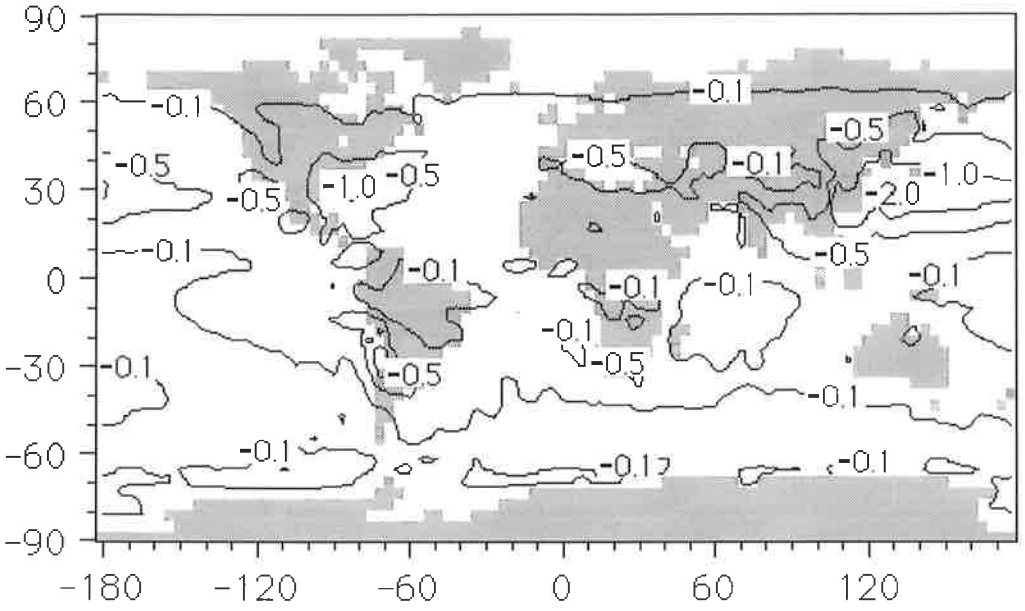

b)

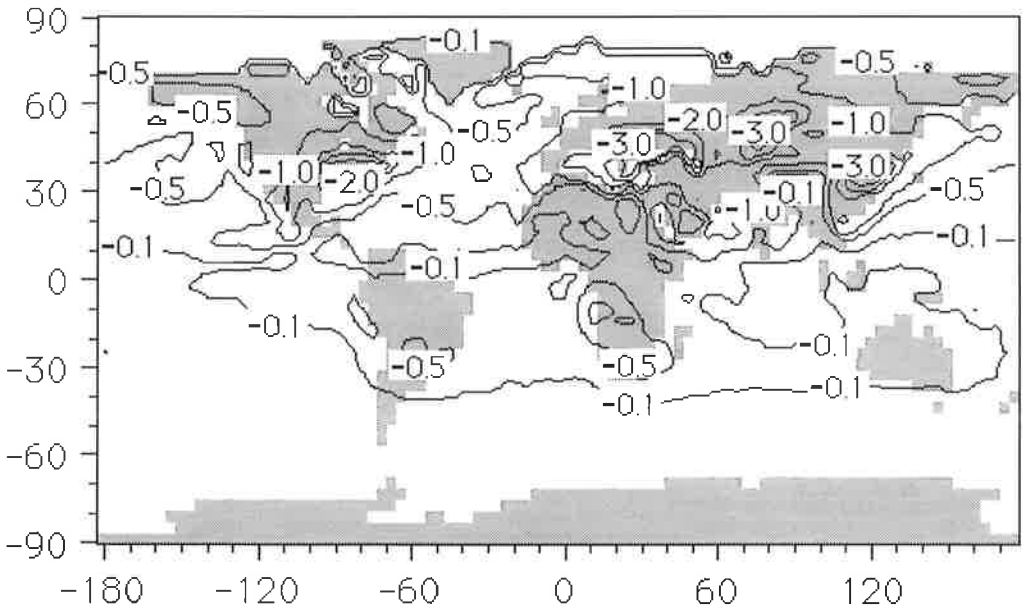

Figure 4. Monthly mean direct anthropogenic forcing in [W m^{-2}].
Contour lines: -0.1, -0,5, -1..0, -1.5, -2.0, -3.0, -4.0
a) January
b) July

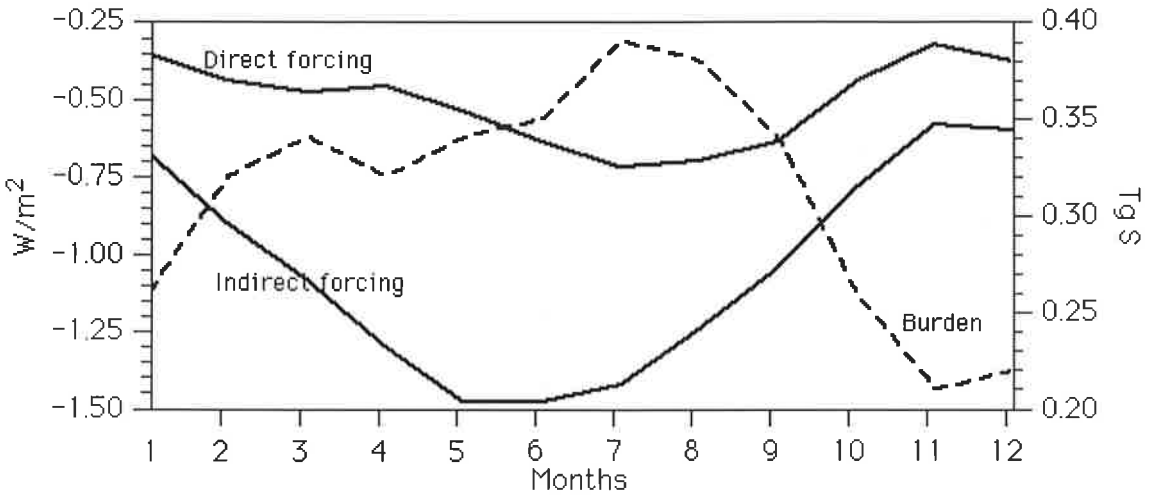

Figure 5. Monthly mean anthropogenic sulfate burden [Tg S] and direct and indirect forcing [W m^{-2}] on the northern hemisphere.

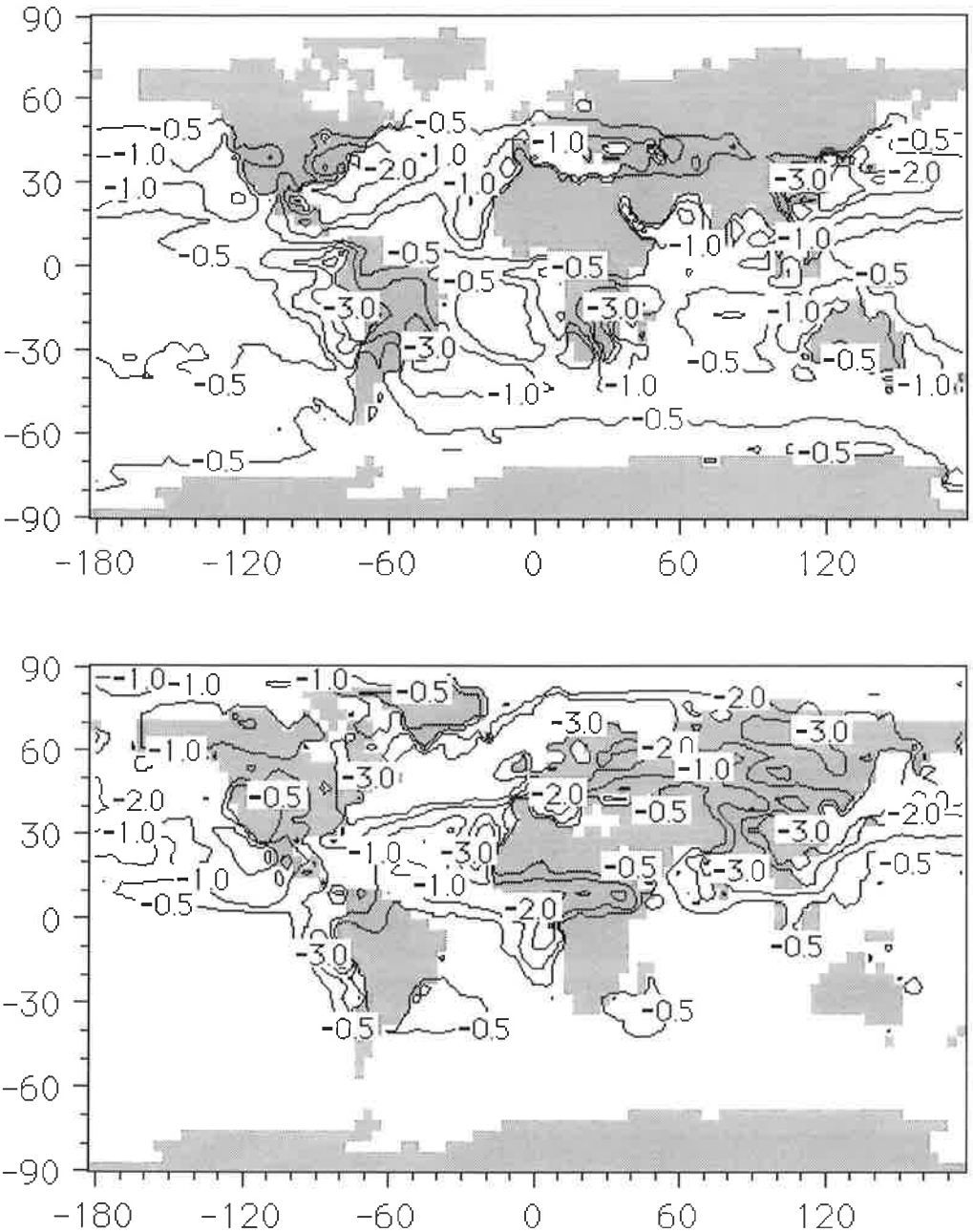

Figure 6. Monthly mean indirect anthropogenic sulfate forcing [W m^{-2}].
Contour lines: -0.5, -1.0, -2.0, -3.0, -4.0
a) January
b) July